Pure Appl. Geophys.
© 2019 Springer Nature Switzerland AG
https://doi.org/10.1007/s00024-019-02331-z

Pure and Applied Geophysics

Trends of Global Seismic Noise Properties in Connection to Irregularity of Earth's Rotation

Alexey Lyubushin[1]

Abstract—The properties of continuous records of low-frequency seismic noise on a global network consisting of 229 broadband seismic stations located around the world are considered. Changes in the properties of seismic noise, estimated daily for the time interval from the beginning of 1997 to the end of February 2019, are investigated. We consider the generalized Hurst exponent, the singularity spectrum support width, the entropy of the wavelet coefficients, and wavelet-based Donoho–Johnstone index. For the centers of 50 clusters of seismic stations, the average values of these 4 statistics from the 5 nearest operational stations are calculated daily. As a result, 4 multidimensional time series with a dimension of 50 are obtained with a time step of 1 day for more than 22 years of measurements. Average daily values of the noise properties studied, calculated over all cluster centers, have piecewise linear trends, the break point of which is estimated by the principal component method as mid-2003. After the break point, the average values of generalized Hurst exponent, singularity spectrum support width and Donoho–Johnstone index the parameters decrease whereas the entropy increases. This is interpreted as a simplification of the noise structure which is typical for areas of high seismic hazard. Trends in average noise properties after 2003 are accompanied by a linear increase with imposed 3-years quasi-periodic fluctuations in the average value of pairwise correlation coefficients between the values in cluster centers when evaluated in a sliding time window with a length of 1 year. It is hypothesized that the simultaneous simplification of the structure of global seismic noise, an increase in its spatial correlation and an increase in the intensity of the strongest earthquakes in the world after the end of 2004 is a single process associated with the irregularity of the Earth's rotation. To confirm this hypothesis, a change in the coherence spectrum between the first principal component of the seismic noise properties and the time series of the length of day is estimated.

Key words: Seismic noise, multifractals, wavelet-based entropy, wavelet-based Donoho–Johnstone index, trends, principal components, correlations, length of day, coherence.

1. Introduction

Seismic noise in various frequency ranges is one of the most frequently studied geophysical research topics. This is due to the presence of numerous regional and global seismic networks, a well-developed practice of seismic observations and the availability of databases. The wide distribution of high-frequency microseismic observations is due to the relative simplicity and mobility of measuring instruments without stringent requirements for the long-term stability of sensors, which cannot be ignored in tasks of low-frequency geophysical monitoring.

The results of studies of seismic noise of natural and industrial origin in the frequency range of 0.01–16 Hz are presented in the article McNamara and Buland (2004). It focuses on the temporal (daily and seasonal) and spatial distribution of the parameters of the estimated power spectra. Similar research questions on the composition of high-frequency microseisms are presented in Koper and de Foy (2008) and Koper et al. (2010). Atmospheric and oceanic waves are the main source of seismic noise energy for large periods. The article Berger et al. (2004) provides an overview of the results obtained using IRIS broadband seismic data. The oceanic origin of seismic noise with periods ranging from 5 to 40 s was established in Stehly et al. (2006). Seismic noise with periods of 100–500 s is generated by both weak earthquakes and processes in the atmosphere and ocean (Friedrich et al. 1998; Kobayashi and Nishida 1998; Tanimoto 2001, 2005; Ardhuin et al. 2011). Climate change is also reflected in variations in the temporal and spatial properties of low-frequency seismic noise (Aster et al. 2008; Grevemeyer et al. 2000; Kedar et al. 2008; Schimmel et al. 2011).

[1] Institute of Physics of the Earth, Russian Academy of Sciences, Moscow, Russia. E-mail: lyubushin@yandex.ru

Published online: 23 September 2019

Assuming that the main source of energy for the global seismic background of the Earth is earthquakes, estimates show that to maintain the observed amount of energy, at least one earthquake of magnitude 6 must occur daily. However, the total contribution of all weak earthquakes, according to the Gutenberg–Richter law, is one or two orders of magnitude less than the real energy of constant seismic noise. As a result of such estimates, it was concluded that cyclone motions in the atmosphere and the effect of waves on the shelf and coast make the main contribution to the low-frequency seismic noise energy (Rhie and Romanowicz 2004, 2006; Fukao et al. 2010; Nishida et al. 2008, 2009).

Considering the earth's crust as the medium of propagation of seismic waves from sources external to it (ocean and atmosphere), we assume that the processes inside the earth's crust are reflected in changes in the statistical properties of seismic noise. Thus, changes in noise properties can be a source of important information about changes in the crust associated with the seismic process and the preparation of strong earthquakes (Lyubushin 2018a, b).

2. Seismic Noise Data

The seismic records were taken by requests to Incorporated Research Institutions for Seismology (IRIS) data base by the address http://www.iris.edu/forms/webrequest/ from 229 seismic stations of 3 global broadband seismic networks:

Global Seismographic Network: http://www.iris.edu/mda/_GSN.

GEOSCOPE: http://www.iris.edu/mda/G.

GEOFON: http://www.iris.edu/mda/GE.

Vertical components with sampling rate 1 Hz (LHZ-records) were downloaded for more than 22 years of observation since 01 Jan 1997 up to 28 Feb 2019. The initial LHZ-records were transformed to sampling time step 1 min by calculating mean values within successive time intervals of the length 60 s. A further analysis is based on estimating statistical properties of low-frequency seismic noise waveforms (periods exceeding 2 min) within successive daily time intervals of the length 1440 samples with time step 1 min.

Let us introduce the so-called reference points—some centers with respect to which the average values of various seismic noise parameters from a given number of the nearest operational stations will be calculated. We choose the number of the nearest stations to be 5, and the number of reference points to be 50. We select the locations of the reference points as the centers of 50 clusters found by the hierarchical method of clustering the positions of seismic stations using the "farthest neighbor". Figure 1 shows the positions of 229 seismic stations and 50 reference points. The choice of farthest neighbor method for clustering seismic stations positions is following from its property for extracting compact clusters (Duda et al. 2000).

Each reference point has its own "area of influence", which includes the nearest 5 operable stations. Depending on the operability of the stations in the current time window, this area constantly pulsates and changes its size. In order to roughly estimate the size of the areas of influence of each reference point, you can use the partition of the surface of the globe into Voronoi polygons, which are presented in Fig. 1.

3. Seismic Noise Statistics

We will analyze 4 properties of seismic noise calculated in adjacent time fragments of 1 day length (1440 counts with a time step of 1 min). Below are descriptions of the statistics used.

Minimum normalized entropy En of wavelet coefficients En. Let $x(t)$ be some finite sample of a certain random signal and let $t = 1, \ldots, N$ be the index that enumerates the successive data points (the discrete time). We determine the normalized entropy of the finite sample by the following formula:

$$En = -\sum_{k=1}^{N} p_k \cdot \log(p_k)/\log(N), \quad p_k = c_k^2 / \sum_{j=1}^{N} c_j^2, \quad 0 \le En \le 1. \tag{1}$$

Here, c_k, $k = 1, N$ are the coefficients of the orthogonal wavelet decomposition with certain basis. Below we used 17 orthogonal Daubechies wavelets: ten ordinary bases with minimal support width with

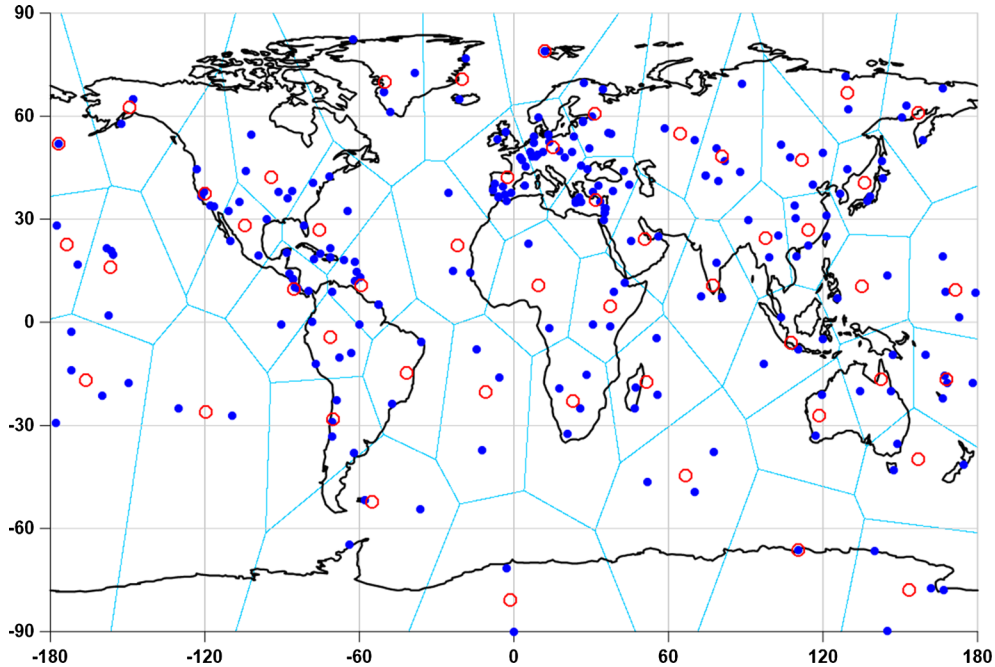

Figure 1
Blue points present positions of 229 broadband seismic stations, red circles give positions of 50 reference points which were defined as centers of clusters from clustering of stations positions using hierarchical farthest-neighbor clustering algorithm. Light-blue lines present Voronoi polygons

1–10 vanishing moments and seven the so called Daubechies symlets (Mallat 1999) with 4–10 vanishing moments. For each basis, the normalized entropy of the distribution of squared coefficients (1) was calculated and the basis that provides the minimum of quantity (1) was determined. We note that due to the orthogonality of wavelet transform, the sum of squared coefficients is equal to the variance (energy) of the signal $x(t)$. Thus, quantity (1) calculates the entropy of energy distribution of the oscillations on the different frequency and time scales.

Minimum normalized entropy *En* was suggested in Lyubushin (2012) and was used for investigating seismic noise properties in Lyubushin (2013, 2014a, b). This entropy measure has some common features with multiscale entropy which was introduced in Costa et al. (2003, 2005) for analysis of time series. In particular orthogonal wavelet transform of the signal, which is used in (1), is multiscale as well because it provides decomposition into discrete dyadic time–frequency "atoms" with energy which is equal to c_k^2.

Donoho–Johnstone index γ. After the wavelet basis is determined for a given signal from the minimum entropy condition, we can find the set of the wavelet coefficients which are smallest by the absolute value. In wavelet filtering, these coefficients can be zeroed before the inverse wavelet transform in order to "reduce the noise" (Donoho and Johnstone 1995; Mallat 1999). We assume that the noise is mainly concentrated in the variations at the first detail level. Due to the orthogonality of wavelet transform, the variance of the wavelet coefficients is equal to the variance of the initial signal. Thus, we estimate the standard deviation of the noise as the standard deviation of the wavelet coefficients at the first level of detail. This estimate should be stable, i.e. insensitive to the outliers in the values of the wavelet coefficients at the first level. For this purpose we can use the robust median estimate of standard deviation for a normal random quantity:

$$\sigma = med\left\{|c_k^{(1)}|, k = 1, \ldots, N/2\right\}/0.6745 \qquad (2)$$

where $c_k^{(1)}$ are the wavelet coefficients at the first level of detail and $N/2$ is the number of these coefficients. The formula (2) is the consequence of the relation between median *Med* and standard deviation σ for Gaussian random value with zero mean: $Med \approx 0.6745 \cdot \sigma$. The estimate of standard deviation σ from formula (2) determines the quantity $\sigma\sqrt{2 \cdot \ln N}$ as a "natural" threshold for separating the noise wavelet coefficients. The quantity $\sigma\sqrt{2 \cdot \ln N}$ is known in wavelet analysis as the Donoho–Johnstone threshold and the expression for this quantity is based on the formula for asymptotic probability of maximal deviations of Gaussian white noise (Mallat 1999). As a result, it is possible to determine the dimensionless characteristic of the signal γ, $0 < \gamma < 1$ as the ratio of the number of the most informative wavelet coefficients for which inequality $|c_k| > \sigma\sqrt{2 \cdot \ln N}$ is satisfied to the total number N of all the wavelet coefficients. Formally, the larger the index γ, the more informative (the less noisy) the signal.

Multifractal parameters $\Delta\alpha$ *and* α^*. Let $x(t)$ be a random signal. Let us define its measure of variability $\mu_X(t, \delta)$ on the time interval $[t, t + \delta]$ as the difference between maximum and minimum values $\mu_x(t, \delta) = \max_{t \le u \le t+\delta} x(u) - \min_{t \le u \le t+\delta} x(u)$ and calculate the mean value of its power degree q: $M(\delta, q) = M[(\mu_x(t, \delta))^q]$. A random signal is scale-invariant (Taqqu 1988) if $M(\delta, q) \sim \delta^{\rho(q)}$ when $\delta \to 0$, that is, the following limit exists:

$$\rho(q) = \lim_{\delta \to 0}(\ln M(\delta, q)/\ln \delta) \qquad (3)$$

If $\rho(q)$ is a linear function $\rho(q) = Hq$, where $H = const$, $0 < H < 1$, the process is monofractal. In the case where $\rho(q)$ is a nonlinear concave function of q, the signal is multifractal. To estimate the value of $\rho(q)$ using a finite sample $x(t)$, $t = 0, 1, \ldots, N - 1$ we used the method, which is based on the approach of detrended fluctuation analysis (DFA) (Kantelhardt et al. 2002). Let us split the entire time series into non-overlapping intervals of length s:

$$I_k^{(s)} = \{t : \ 1 + (k-1)s \le t \le ks, \quad k = 1, \ldots, [N/s]\} \qquad (4)$$

and let

$$y_k^{(s)}(t) = x((k-1)s + t), \quad t = 1, \ldots, s \qquad (5)$$

be a part of the signal $x(t)$, corresponding to interval $I_k^{(s)}$. Let $p_k^{(s,m)}(t)$ be a polynomial of the order m, best fitted to the signal $y_k^{(s)}(t)$. Let us consider the deflections from the local trend:

$$\Delta y_k^{(s,m)}(t) = y_k^{(s)}(t) - p_k^{(s,m)}(t), \quad t = 1, \ldots, s \qquad (6)$$

and calculate the values

$$Z^{(m)}(q, s) = \left(\sum_{k=1}^{[N/s]} (\max_{1 \le t \le s} \Delta y_k^{(s,m)}(t) - \min_{1 \le t \le s} \Delta y_k^{(s,m)}(t))^q \Big/ [N/s]\right)^{1/q} \qquad (7)$$

that can be regarded as the estimate of $(M(\delta_s, q))^{1/q}$. Let us define the function $h(q)$ as a coefficient of linear regression between $\ln(Z^{(m)}(q, s))$ and $\ln(s)$: $Z^{(m)}(q, s) \sim s^{h(q)}$ fitted for scales range $s_{\min} \le s \le s_{\max}$. It is evident that $\rho(q) = qh(q)$ and, for a monofractal signal, $h(q) = H = const$. The multifractal singularity spectrum $F(\alpha)$ is equal to the fractal dimensionality of the set of time moments t for which the Hölder–Lipschitz exponent is equal to α i.e. for which $|x(t + \delta) - x(t)| \sim |\delta|^{\alpha}$, $\delta \to 0$ (Feder 1988). The singularity spectrum can be estimated using the standard multifractal formalism, which consists in calculating the Gibbs sum:

$$W(q, s) = \sum_{k=1}^{[N/s]} \left(\max_{1 \le t \le s} \Delta y_k^{(s,m)}(t) - \min_{1 \le t \le s} \Delta y_k^{(s,m)}(t)\right)^q \qquad (8)$$

and in estimating the mass exponent $\tau(q)$ from the condition $W(q, s) \sim s^{\tau(q)}$. From (7) it follows that $\tau(q) = \rho(q) - 1 = qh(q) - 1$. In the next step, the spectrum $F(\alpha)$ is calculated with the Legendre transform:

$$F(\alpha) = \max\{\min_q(\alpha q - \tau(q)), 0\} \qquad (9)$$

If the singularity spectrum $F(\alpha)$ is estimated in a moving window, its evolution can give useful

information on the variations in the structure of the "chaotic" pulsations of the series. In particular, the position and width of the support of the spectrum $F(\alpha)$, i.e., the values $\alpha_{\min}, \alpha_{\max}, \quad \Delta\alpha = \alpha_{\max} - \alpha_{\min}$, and α^*, such that $F(\alpha^*) = \max_\alpha F(\alpha)$, are characteristics of the noisy signal. The value α^* can be called a generalized Hurst exponent and it gives the most typical value of Lipschitz-Holder exponent. Parameter $\Delta\alpha$, singularity spectrum support width, could be regarded as a measure of variety of stochastic behavior. In the case of a monofractal signal, the quantity $\Delta\alpha$ should vanish and $\alpha^* = H$. Usually $F(\alpha^*) = 1$, but there exist time windows for which $F(\alpha^*) < 1$. Estimates of minimum Hölder–Lipschitz exponent $\alpha_{\min}$ are mainly positive. Nevertheless negative values of $\alpha_{\min}$ are quite possible as well (Telesca et al. 2005; Currenti et al. 2005; Telesca and Lovallo 2011; Chandrasekhar et al. 2016) for time fragments which are characterized by high-amplitudes spikes and steps.

Multifractal analysis is a rather popular tool in geophysical studies (Ramirez-Rojas et al. 2004; Ida et al. 2005; Currenti et al. 2005; Telesca et al. 2005; Chandrasekhar et al. 2016). Natural time analysis (Varotsos et al. 2011) has a long history of its applications to geophysical problems by using multifractal and entropy toolbox. The paper (Varotsos et al. (2003a)) is devoted to investigating seismic electric signals activities (SES) by using multifractal detrended fluctuation analysis (DFA) in combination with natural time approach. In Varotsos et al. (2003b) SES was studied using natural time based entropy. In Sarlis et al. (2018) a multi-scale analysis of global seismic process is presented which is based on applying a large number of methods which are based on fractal and multi-fractal approaches and using of natural time technique. In the papers (Lyubushin 2009, 2010a, b, 2011, 2012, 2013, 2014a, b, 2015, 2018b, c) estimates of multifractal properties $\Delta\alpha$, α^* and $\alpha_{\min}$ of low-frequency seismic noise were used for the purposes of earthquake prediction and dynamic estimate of seismic danger.

4. Trends of Noise Parameters

Let's consider a sequence of adjacent time windows of a length of 1440 samples with a time step of 1 min, that is, a length of 1 day. In each time window, we calculate the values of the 4 noise statistics *En*, γ, α^* and $\Delta\alpha$ described above. At the same time, we will exclude trends within each window by an 8^{th} order polynomial. Subtracting trends eliminates the influence of Earth tides. A station is considered operable within the considered time window if its records inside the window do not contain gaps. For each reference point and for each time window, we find 5 nearest operational stations, and then assign a reference point to the value of one or another of the 4 statistics, equal to the average value from the 5 nearest operating-state stations. Thus, for each reference point we get 4 time series with a time step of 1 day.

Figure 2 presents graphs of such time series for the mean values of the generalized Hurst exponent α^* at 50 reference points from 5 nearest operable seismic stations. Similar series of graphics could be plotted for other three noise parameters. At first glance these time series look very chaotic. For getting their general features let's calculate mean values by averaging daily values from all 50 reference points. Graphs of these mean values are presented at Fig. 3. The main feature of the graphs of average values is the existence of time points separating fragments with different linear trends. For all four parameters, there are points for which the slope of the linear trend, fitted to the average values to the left and right of the point, differs significantly. In Fig. 3, bold green lines show graphs of continuous piecewise linear trends with one corner point, the position of which is found automatically from the condition of minimum variance of the remainder after eliminating such a broken trend. Time marks are given in fractional years, i.e. share of any year corresponds to the number of the day divided by the whole number of days within year. In brackets a usual data is given in the format year.month.day. The next values of linear trends corner points were found: α^*—2003.699 (2003.09.12); $\Delta\alpha$—2003.466 (2003.06.19); *En*—2004.79 (2004.10.15); γ—2004.566 (2004.07.25).

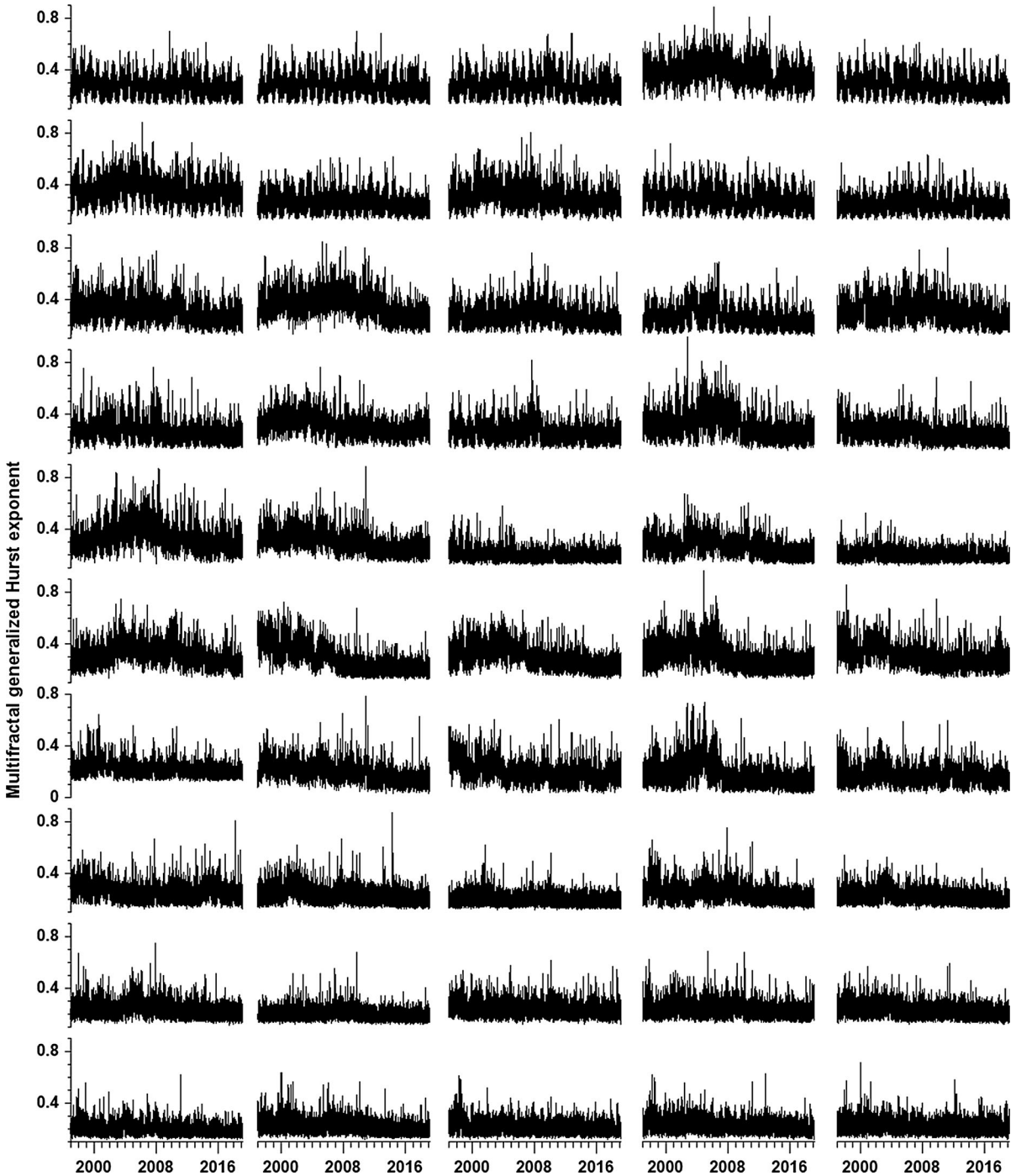

Figure 2
Graphs of daily values of generalized Hurst exponents α^* which were calculated for each of 50 centers of stations clusters (reference points) as mean values from 5 nearest operable stations. All graphs are plotted in the same scale by Y-axes

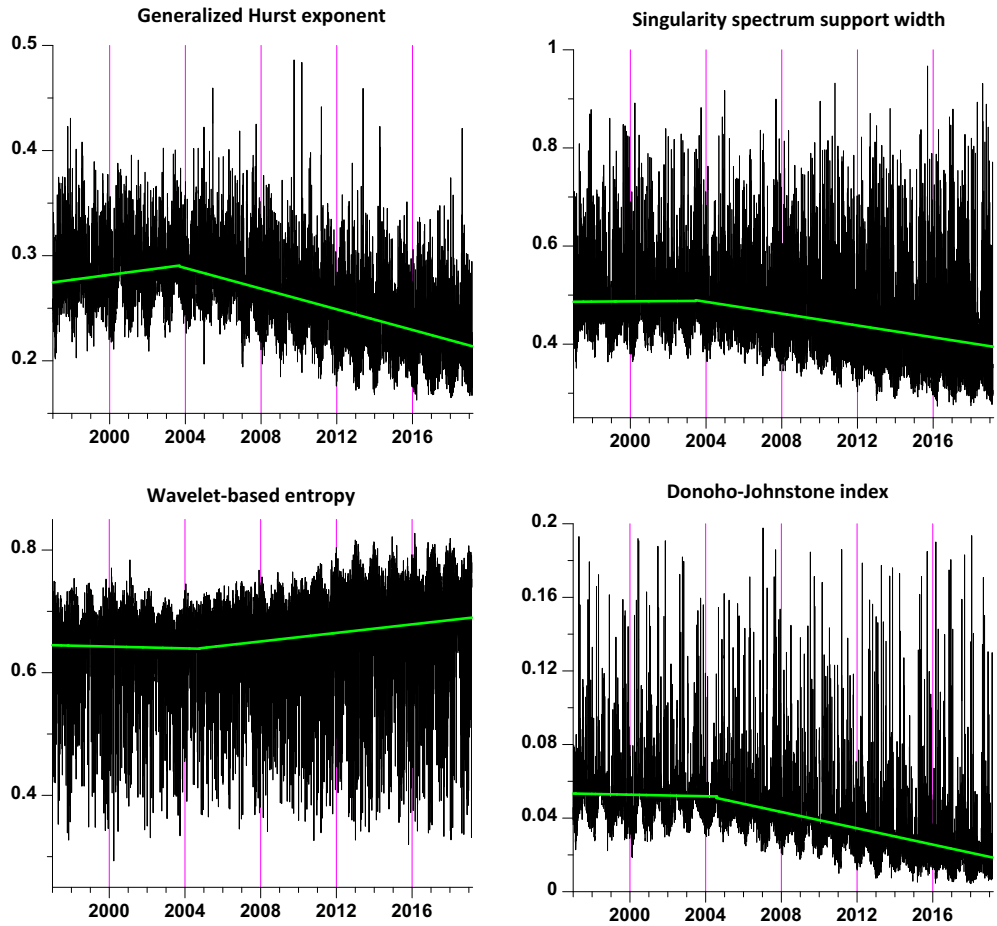

Figure 3
Graphs of daily values of 4 seismic noise statistics averaged from values in 50 reference points (centers of seismic stations clusters), bold green lines present continuous piecewise linear trends with corner points

Thus, the positions of the corner points of the continuous piecewise linear trends are rather close to each other: mean value of corner point's positions is 2004.13 (2004.02.17) with standard deviation 0.646 (236 days). Method of principal components (PC) (Jolliffe 1986) gives other way for obtaining some mean position of corners point, which is based on extracting the most informative common features from the curves. Let's calculate the first principal component of the four mean values presented in Fig. 3. Its graph is presented at the Fig. 4 and we can notice the same main peculiarity of its temporal behavior: the existence of linear trend corner point. The position of first principal component corner point is estimated as 2003.726 (2003.09.22). This time we selected as the change point for properties of seismic noise.

Another issue of interest is the correlation of variations in the properties of seismic noise obtained for 50 reference points located throughout the world. To determine the correlation properties, we consider a sliding time window with a length of 1 year (365 days) and for each window position we calculate the absolute values of the pairwise correlations between the values of properties at all reference points. For 50 reference points there will be 1225 such correlations. Next, we calculate their average, which will give us the average measure of global correlations of seismic noise properties. If we construct the mean absolute correlation values depending

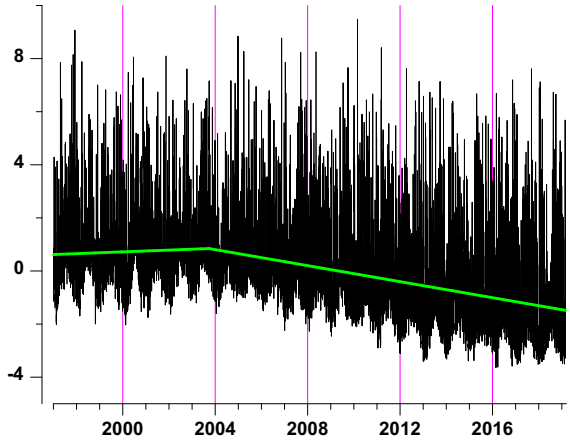

Figure 4
Graph of first principal component of 4 daily properties of global seismic noise presented at Fig. 3; bold green line presents continuous piecewise linear trend with corner point at time moment 2003.726

on the position of the right-hand end of the sliding time window, we can get an idea of how the correlations change over time.

5. Correlations of Noise Parameters

Figure 5a shows the graphs of the average values of the absolute values of the pairwise correlations for the four statistics used, calculated in a sliding time window of 365 days. It can be seen that these graphs are similar to each other and that they, as well as the average values in Fig. 3, are characterized by the presence of time points, in which the slopes of the linear trends in the right and left of these points changes dramatically. It can also be seen that the point of change in the linear trend for all the mean correlations is about the same. To determine this time point of a trend change for correlations, we calculate the average of all four correlations in Fig. 5a. This average value is represented in Fig. 5b by the black line, and the green line in Fig. 5b is the piecewise linear trend with one corner point, which is found from the condition of minimum residual variance. The trend corner point value for average correlations is estimated as 2003.2.

Thus, since 2003, there has been a rapid increase in global correlations of seismic noise properties. Moreover, quasi-periodic fluctuations are superimposed on the linear growth of correlations. To determine the period of these fluctuations, we exclude the influence of the piecewise linear trend. The result of this operation is shown in Fig. 5c. Next, we calculate the average value of the squares of the wavelet coefficients of the continuous Morlet wavelet transform (Mallat 1999):

$$c(t,a) = \frac{1}{\sqrt{a}} \int_{-\infty}^{+\infty} x(s) \cdot \psi\left(\frac{s-t}{a}\right) ds, \quad a > 0, \qquad \psi(t) = \frac{1}{\pi^{1/4}} \exp(-t^2/2 - i\pi t). \tag{10}$$

The values of $|c(t,a)|^2$ could be interpreted as the energy of oscillation of the signal $x(s)$ at the vidicinity of time moment t with a period a. Wavelet-based Morlet spectrum is calculated as period-dependent mean values of $|c(t,a)|^2$ with respect to all time moments t. Figure 5d presents graph of Morlet spectrum and it is obvious that it has a strong peak at the period 1067 days which is near 2.9 years.

It is possible to sum up the intermediate results of the seismic noise properties:

1. In 2003 the trend of noise properties changes dramatically;
2. In 2003 the trend of global noise correlations changes just as sharply.

It should be noted that after 2003, the trends of seismic noise properties could be characterized as simplifying its structure: a decrease in the singularity spectrum support width $\Delta\alpha$ (the "loss of multifractality"), an increase in entropy En and a decrease in the share of informative wavelet coefficients γ.

The question arises: what could be the cause of such abrupt changes in the properties of seismic noise, considered on a global scale? As a hypothesis, we consider the influence of the irregularity of the Earth's rotation.

6. Length of Day Time Series and Its Measure of Non-stationarity

Length of day (LOD) time series is an indicator of irregularity of Earth's rotation and it could be

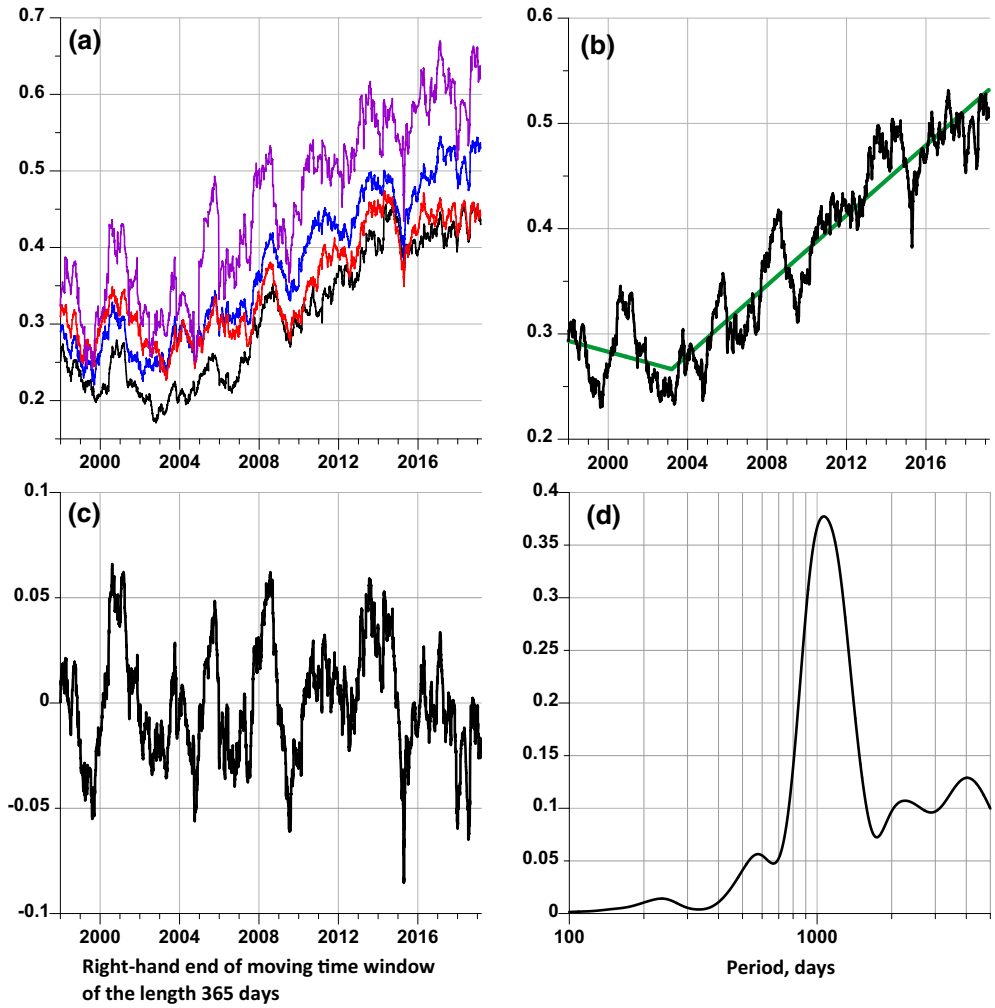

Figure 5

a Graphs of mean values of absolute pairwise correlation coefficients between 4 daily seismic noise parameters estimated within 50 reference points all over the world in moving time window of the length 365 days: black line—for generalized Hurst exponent α^*, blue line—for singularity spectrum support width $\Delta\alpha$, red line—for wavelet-based minimum entropy and purple line—for wavelet-based DJ index γ. Black line at **b** presents mean correlation coefficient from all coefficients at the left panel. Green line at **b** presents continuous piecewise linear trend with corner point at 2003.2, which was found from minimum of residual variance. **c** Residuals after removing broken linear trend at **b**. **d** Graph of Morlet wavelet spectrum of the detrended mean correlation coefficient at **c** with maximum at the period 1067 days $\approx$ 2.9 years

downloaded from the beginning of 1962 till now by the address https://hpiers.obspm.fr/iers/eop/eopc04/eopc04.62-now. We used the fragment of LOD time series which is simultaneous to the used seismic records. We are interesting in the effects of the nonstationary behavior of LOD time series, since they can be triggers for changing the properties of global seismic noise. Let's describe the method for constructing measure of non-stationarity.

Simple orthogonal wavelet decomposition presents each signal $z(t), \quad t = 1, \ldots, N$ as a sum of its detail levels components (Mallat 1999):

$$z(t) = a_1^{(m)} + \sum_{\beta=1}^{m} z^{(\beta)}(t) \qquad (11)$$

where $z^{(\beta)}(t)$ is the component of the signal belonging to the detail level of the number β and $a_1^{(m)}$ is a constant proportional to the mean of the sample, m is

the general number of detail levels. At a sufficiently large number N of samples, the spectrum of component $z^{(\beta)}(t)$ is localized mainly within the frequency band:

$$[\Omega_{\min}^{(\beta)}, \Omega_{\max}^{(\beta)}] = [2\pi/(2^{(\beta+1)}\Delta t),\ 2\pi/(2^{\beta}\Delta t)] \quad (12)$$

where Δt is the length of the sampling time interval.The orthogonal wavelet-packet expansion of the signal can be, by analogy with formula (11), written as the sum:

$$z(t) = a_1^{(m)} + \sum_{\beta=m_q+1}^{m} z^{(\beta)}(t) + \sum_{\beta=1}^{m_q}\sum_{j=1}^{q} z^{(\beta,j)}(t). \quad (13)$$

The quantity q can be equal to 2, 4, 8, …, i.e., $q = 2^r,\ r = 1, 2, 3, \ldots$, and it controls the number of sublevels into which an ordinary detail level is split. For a given value of q, the maximum number $m_q < m$ of the detail level β that can be split is determined from the condition that this level must contain at least q wavelet coefficients. The components $z^{(\beta,j)}(t)$ are frequency-ordered and split frequency band (12) of detail level β into q equal parts. Thus, the spectrum of signal $z^{(\beta,j)}(t)$ is localized mainly in the frequency band:

$$\left[\Omega_{\min}^{(\beta,j)}, \Omega_{\max}^{(\beta,j)}\right], \quad \Omega_{\min}^{(\beta,j)} = \Omega_{\min}^{(\beta)} + (j-1)\cdot\Delta\Omega^{(\beta)},$$
$$j = 1, \ldots, q;$$
$$\Omega_{\max}^{(\beta,j)} = \Omega_{\min}^{(\beta,j)} + \Delta\Omega^{(\beta)}, \Delta\Omega^{(\beta)} = (\Omega_{\max}^{(\beta)} - \Omega_{\min}^{(\beta)})/q \quad (14)$$

Let $x_j(t) = z^{(1,j)}(t)$, $x_{8+j}(t) = z^{(2,j)}(t)$, $1 \le j \le 8$, be wavelet-packet components of LOD time series from the formula (13) for the first two detail levels with splitting each level into $q = 8$ sublevels, where j is an integer number of wavelet-packet sublevel, $j_0 \le j \le j_1$. For our case $j_0 = 1$, $j_1 = 16$, $\Delta t = 1$, indexes $j = 1, \ldots, 8$ correspond to sublevels of the first detail level, whereas $j = 9, \ldots, 16$—to sublevels of second detail level. Let's perform preliminary normalizing operation:

$$y_j(t) = x_j(t) \Big/ \max_t |x_j(t)|. \quad (15)$$

Let s be a center of sliding time window of the length $(2m_j + 1)$ samples, where $m_j = [\tau_j]$, $\tau_j = 2\pi \Big/ \Omega_{\min}^{(1,j)}$ and $\tau_{8+j} = 2\pi \Big/ \Omega_{\min}^{(2,j)}$, $1 \le j \le 8$, are values of maximum periods corresponding to wavelet-packet frequency bands in the formula (14). Let's calculate sums of squared amplitudes of normalized wavelet-packet components $y_j(t)$ in the left-hand and right-hand vicinities of the moving central point s:

$$Z_{\text{Left}}^{(j)}(s) = \sum_{t=s-m_j}^{s-1} |y_j(t)|^2, \quad Z_{\text{Right}}^{(j)}(s) = \sum_{t=s+1}^{s+m_j} |y_j(t)|^2 \quad (16)$$

and calculate their mean difference:

$$\Delta Z^{(j)}(s) = \left(Z_{\text{Left}}^{(j)}(s) - Z_{\text{Right}}^{(j)}(s)\right)/m_j. \quad (17)$$

A wavelet-packet-based measure of non-stationarity is defined by the formula:

$$r^2(s) = \sum_{j=j_0}^{j_1} |\Delta Z^{(j)}(s)|^2/(j_1 - j_0 + 1). \quad (18)$$

This measure is defined for time points s satisfying condition $1 + m_{j_1} \le s \le N - m_{j_1}$. The orthogonal wavelet basis function was chosen as Daubechies symlet with 9 vanishing moment using principle of minimum entropy of squared wavelet coefficients (Mallat 1999).

Figure 6 shows the graphs of the LOD time-series, its wavelet-packet decomposition for the first 2 levels of detail and the measure (18), which collects together the effects of non-stationary behavior from all sublevels, many of which are seen visually in the 16 graphs of the series Fig. 6b. In Fig. 6c it is clear that the measure of non-stationarity has 3 groups of strong bursts of its values with instants of time of maximal surge in each group 2000.745, 2002.388 and 2006.155, and the second burst at time 2002.388 is maximal.

The behavior of the non-stationarity measure on Fig. 6c provides us a foundation for hypothesis that the first 2 bursts of the measure (18) of the irregular rotation of the Earth at times 2000.745 and, especially, the maximum spike in time 2002.388 triggered changes in the trends of global seismic noise properties in 2003 (Fig. 4), and also initiated a strong trend of increasing their correlations (Fig. 5a, b).

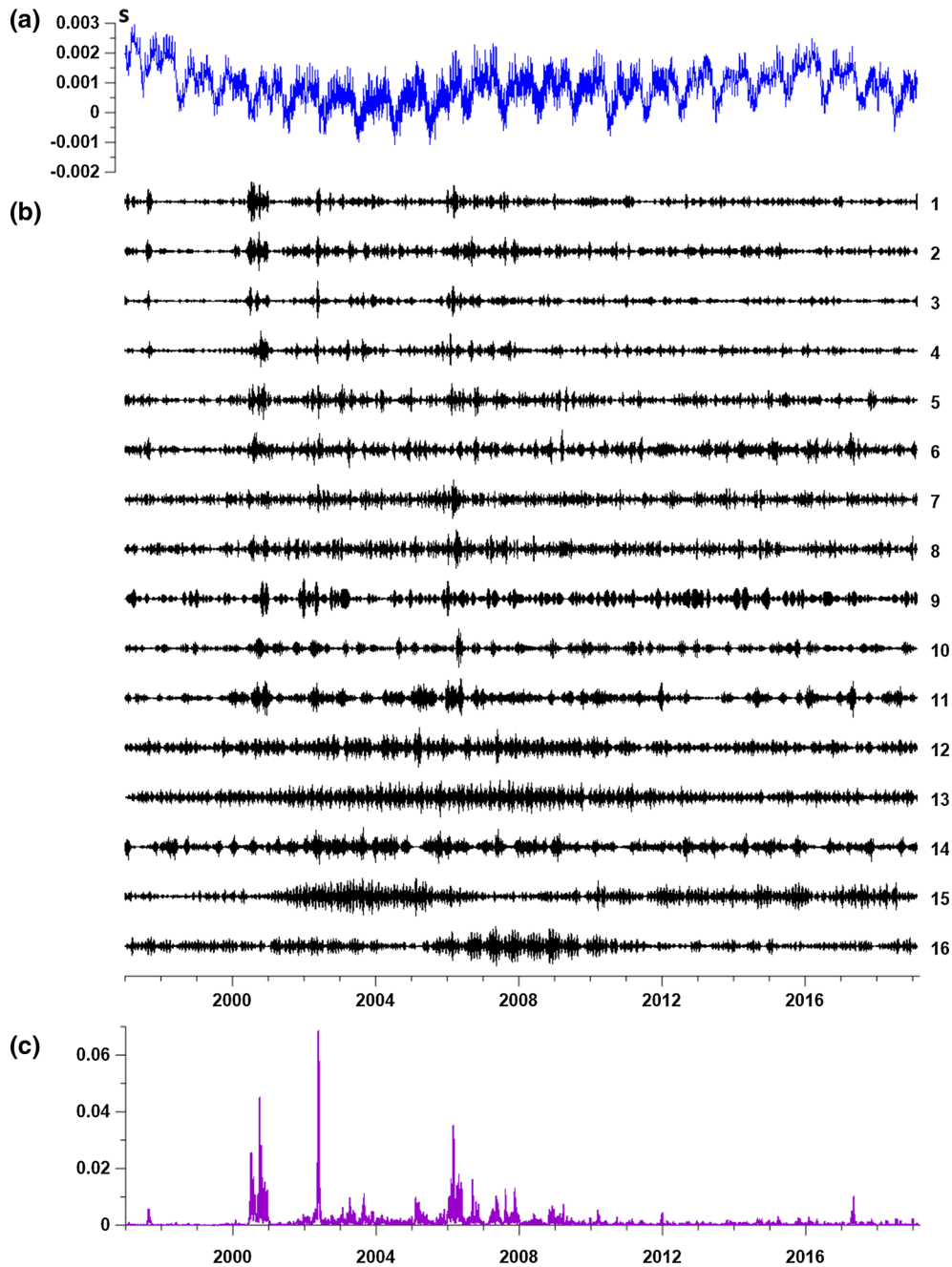

Figure 6

a Blue line—graph of LOD time series (seconds) since beginning of 1997 up to Feb 28, 2019; **b** 16 graphs by black lines—LOD normalized wavelet-packet components $y_j(t), \quad j = 1, \ldots, 16$ of first 2 detail levels with splitting each level into 8 sublevels; **c** purple line—graph of measure of non-stationarity (18)

7. Coherence Spectrum Between LOD and Seismic Noise Properties

There is a possibility to establish direct connection between LOD time series and seismic noise properties. For this purpose we can estimate squared coherence spectrum between LOD and first principal component (PC) of noise properties (Fig. 4) in a moving time window and obtain a time–frequency 2D diagram of its evolution. For estimating coherence we will use parametric vector autoregression model because it possesses more high frequency resolution in comparison with non-parametric methods using Fourier transform and further smoothing of periodograms (Marple 1987).

A vector autoregression model for m-dimensional time series (in our case $m = 2$) is defined by formula:

$$U(t) + \sum_{k=1}^{p} A_k \, U(t-k) = e(t) \qquad (19)$$

where t is time index within current time window with the time coordinate τ, $U(t)$ is the piece of m-dimensional time series corresponding to the current time window, p is an autoregression order, A_k are matrices of autoregression coefficients of the size $m \times m$, $e(t)$ is m-dimensional residual signal with zero mean and covariance matrix $\Phi = M\{e(t)e^T(t)\}$. Matrices A_k and Φ are defined in each time window using Durbin–Levinson procedure (Marple 1987) and the spectral matrix is calculated using the formula:

$$\begin{aligned} S(\omega) &= F^{-1}(\omega) \cdot \Phi \cdot F^{-H}(\omega), \\ F(\omega) &= I + \sum_{k=1}^{p} A_k \cdot \exp(-i\omega k) \end{aligned} \qquad (20)$$

where I is a unit matrix of the size $m \times m$, H is the sign of Hermitian conjunctions. We applied the model (19) for the case when $m = 2$ within time windows of the length $L = 365$ daily samples (1 year) with mutual shift 7 days. We used autoregression order $p = 5$ in the Eq. (19).

The squared coherence spectrum is calculated by formula

$$C^2(\omega) = |S_{12}(\omega)|^2 / (S_{11}(\omega) \cdot S_{22}(\omega)) \qquad (21)$$

where $S_{11}(\omega)$, $S_{22}(\omega)$ are diagonal elements and $S_{12}(\omega) = S_{21}^*(\omega)$ are non-diagonal elements of the matrix (20) of the size 2×2. The function (21) could be interpreted as frequency-dependent squared correlation coefficient between 2 signals, $0 \le C^2(\omega) \le 1$.

Figure 7 presents results of estimating evolution of squared coherence spectrum (21) in moving time window of the length 365 days using vector autoregression model (19–20). Time–frequency diagram at Fig. 7b shows that coherence is concentrated in narrow band with boundary periods 8 and 19 days and maximum of mean coherence corresponds to period 13 days (Fig. 7c).

Graph at Fig. 7a presents the maximum values of squared coherence within frequency band with periods from 8 up to 19 days. We see that the most essential maximum corresponds to time interval 2002–2004 what includes time moment of change of seismic noise properties trends (Fig. 4) and time moment of biggest spike of measure of non-stationarity of Earth's rotation irregularity (Fig. 6c). Time interval of changing trend of global correlations at Fig. 5b belongs to the window 2002–2004 as well.

8. Conclusion

Seismic noise is the product of the inner life of the upper shell of the Earth—its crust. The approach of a complex system to a catastrophe is accompanied by a change in the properties of random fluctuations of its parameters and, in particular, in an increase in the radius of correlations of fluctuations (Gilmore 1981; Nicolis and Prigogine 1989). An increase in the spatial radius of correlations is manifested in an increase in the mean value of correlations, as illustrated in the graphs in Fig. 5a, b. Earlier, the effect of increasing the correlation and coherence of fluctuations of global seismic noise parameters was already discovered in the works (Lyubushin 2014b, 2015, 2018a) where it was interpreted as indicator of progressive increasing of global seismic danger after Sumatra mega-earthquake at December 26, 2004. Using of coherence spectra helps to extracting hidden effects of geophysical fields' synchronization. In Filatov and Lyubushin (2019) increasing of multiple coherence measure which is based on using of canonical coherences in combination with fractal analysis was used for extracting seismically active regions in California by analysis of GPS

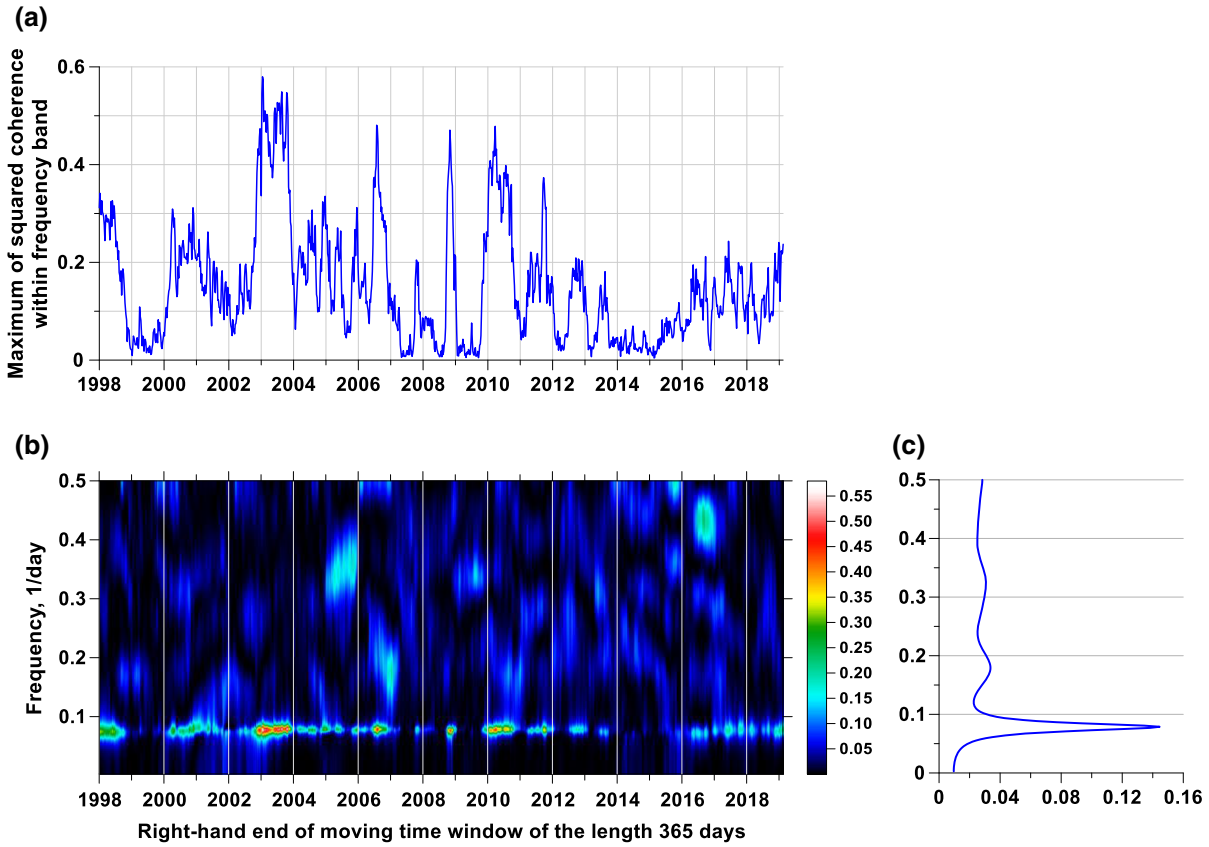

Figure 7

a Maximum of squared coherence spectrum within frequency band with periods from 8 up to 19 days. **b** Squared coherence spectrum between LOD and first principal component of daily mean values of 4 seismic noise properties averaged from 50 reference points all over the world within moving time window of the length 365 days. **c** Coherence spectrum averaged from all time windows

measured Earth's surface tremor. Abrupt simultaneous increasing in 2010–2011 of coherence spectra and mean correlations of daily GPS time series within 9 regions over the world was discovered in Lyubushin (2018b).

In this article, a new effect of seismic noise was discovered—a simplification of its structure, which manifests itself in a change in trends in noise properties after 2003. For example, a decrease in the singularity spectrum support width $\Delta\alpha$ of various biological and medical indicators due to deterioration of health was noted in the works (Ivanov et al. 1999; Humeaua et al. 2008; Dutta et al. 2013). In papers (Lyubushin 2012, 2013, 2014a, 2018a) it was shown that decrease of $\Delta\alpha$ and increase of wavelet-based entropy *En* for seismic noise are typical for regions with increasing seismic danger. In (Pavlov and Anishchenko 2007) it was shown that decrease of $\Delta\alpha$ ("loss of multifractality") has a rather universal character and is observed in physical systems as well as phenomena which are connected with synchronization of behavior of their parts.

Thus, the simplification of the structure of seismic noise and the increase in its synchronization (correlation) are the indicators of the global increase in seismic hazard. Comparison of the distinguished features of the seismic noise properties with LOD time series allows us to suggest that the reason for these changes can be quite rapid changes in the irregularity of the Earth's rotation.

The reason for the uneven rotation of the Earth is currently far from complete clarity. As factors influencing this non-uniformity, one can point to thermodynamic processes in the ocean, atmosphere, and lithosphere, which are accompanied by redistribution of masses, a change in the magnetic field, and

an exchange of angular momentum between the shells. Of these hypothetical factors, the most studied is the effect of the atmosphere, which for the periods from several days to several years is the most intense, affecting the length of the day (Zotov et al. 2017). At the same time, as discussed in the introduction, the process in the atmosphere and the storm waves generated by them in the ocean are the main sources of seismic background energy in the earth's crust. Therefore, as a hypothesis that relates the changes in the properties of the Earth's seismic noise property and the planet's irregular rotation, we can assume that long-period climatic processes, which are reflected in the intensity of the action of the liquid shell on the lithosphere, are a factor combining changes in the length of the day and seismicity. This effect can be either in the form of direct wind pressure on mountain ranges, or in the form of a change in the load on the lithosphere due to melting glaciers, rising sea levels and the intensity of precipitation. Thus, those features of the Earth's global seismic noise that are the subject of data analysis in this article (simplification of the statistical structure and growth of correlations) can be a manifestation of the deep connections between processes in different shells of the planet and climate change (Zotov et al. 2016).

Acknowledgements

The research was supported by the Russian Foundation for Basic Research, Grant no. 18-05-00133, project "Estimation of fluctuations of seismic hazard on the basis of complex analysis of the Earth's ambient noise."

Publisher's Note Springer Nature remains neutral with regard to jurisdictional claims in published maps and institutional affiliations.

References

Ardhuin, F., Stutzmann, E., Schimmel, M., & Mangeney, A. (2011). Ocean wave sources of seismic noise. *Journal of Geophysical Research, 116,* C09004.

Aster, R., McNamara, D., & Bromirski, P. (2008). Multidecadal climate induced variability in microseisms. *Seismological Research Letters, 79,* 194–202.

Berger, J., Davis, P., & Ekstrom, G. (2004). Ambient earth noise: A survey of the global seismographic network. *Journal of Geophysical Research, 2004*(109), B11307.

Chandrasekhar, E., Sanjana, S. P., Gopi, K. S., & Nayana, S. (2016). Multifractal detrended fluctuation analysis of ionospheric total electron content data during solar minimum and maximum. *Journal of Atmospheric and Solar-Terrestrial Physics, 149,* 31–39. https://doi.org/10.1016/j.jastp.2016.09.007.

Costa, M., Goldberger, A. L., & Peng, C.-K. (2005). Multiscale entropy analysis of biological signals. *Physical Review E, 71*(2005), 021906.

Costa, M., Peng, C.-K., Goldberger, A. L., & Hausdorf, J. M. (2003). Multiscale entropy analysis of human gait dynamics. *Physica A, 330*(2003), 53–60.

Currenti, G., del Negro, C., Lapenna, V., & Telesca, L. (2005). Multifractality in local geomagnetic field at Etna volcano, Sicily (southern Italy). *Natural Hazards and Earth System Science, 5,* 555–559.

Donoho, D. L., & Johnstone, I. M. (1995). Adapting to unknown smoothness via wavelet shrinkage. *Journal of American Statistical Association, 90*(432), 1200–1224.

Duda, R. O., Hart, P. E., & Stork, D. G. (2000). *Pattern classification* (p. 680). New York: Wiley-Interscience Publication.

Dutta, S., Ghosh, D., & Chatterjee, S. (2013). Multifractal detrended fluctuation analysis of human gait diseases. *Frontiers in Physiology, 4,* 2013. https://doi.org/10.3389/fphys.2013.00274.

Feder, J. (1988). *Fractals* (p. 284). New York: Plenum Press.

Filatov, D. M., & Lyubushin, A. A. (2019). Precursory analysis of GPS time series for seismic hazard assessment. *Pure and Applied Geophysics*. https://doi.org/10.1007/s00024-018-2079-3.

Friedrich, A., Krüger, F., & Klinge, K. (1998). Ocean-generated microseismic noise located with the Gräfenberg array. *Journal of Seismology, 2*(1), 47–64.

Fukao, Y. K., Nishida, K., & Kobayashi, N. (2010). Seafloor topography, ocean infragravity waves, and background Love and Rayleigh waves. *Journal of Geophysical Research, 115,* B04302.

Gilmore, R. (1981). *Catastrophe theory for scientists and engineers*. New York, NY: Wiley.

Grevemeyer, I., Herber, R., & Essen, H.-H. (2000). Microseismological evidence for a changing wave climate in the northeast Atlantic Ocean. *Nature, 408,* 349–352.

Humeaua, A., Chapeau-Blondeau, F., Rousseau, D., Rousseau, P., Trzepizur, W., & Abraham, P. (2008). Multifractality, sample entropy, and wavelet analyses for age-related changes in the peripheral cardiovascular system: Preliminary results. *Medical Physics, American Association of Physicists in Medicine, 35*(2), 717–727.

Ida, Y., Hayakawa, M., Adalev, A., & Gotoh, K. (2005). Multifractal analysis for the ULF geomagnetic data during the 1993 Guam earthquake. *Nonlinear Processes Geophys., 12,* 157–162.

Ivanov, P Ch., Amaral, L. A. N., Goldberger, A. L., Havlin, S., Rosenblum, M. B., Struzik, Z., et al. (1999). Multifractality in healthy heartbeat dynamics. *Nature, 399,* 461–465.

Jolliffe, I. T. (1986). *Principal component analysis*. Berlin: Springer. https://doi.org/10.1007/b98835.

Kantelhardt, J. W., Zschiegner, S. A., Konscienly-Bunde, E., Havlin, S., Bunde, A., & Stanley, H. E. (2002). Multifractal

detrended fluctuation analysis of nonstationary time series. *Physica A, 316*(1–4), 87–114.

Kedar, S., Longuet-Higgins, M., Webb, F., Graham, N., Clayton, R., & Jones, C. (2008). The origin of deep ocean microseisms in the North Atlantic Ocean. *Proceedings of the Royal Society A, 464,* 777–793.

Kobayashi, N., & Nishida, K. (1998). Continuous excitation of planetary free oscillations by atmospheric disturbances. *Nature, 395,* 357–360.

Koper, K. D., & de Foy, B. (2008). Seasonal anisotropy in short-period seismic noise recorded in South Asia. *Bulletin of the Seismological Society of America, 98,* 3033–3045.

Koper, K. D., Seats, K., & Benz, H. (2010). On the composition of Earth's short-period seismic noise field. *Bulletin of the Seismological Society of America, 100*(2), 606–617.

Lyubushin, A. A. (2009). Synchronization trends and rhythms of multifractal parameters of the field of low-frequency microseisms. *Izvestiya, Physics of the Solid Earth, 45*(5), 381–394. https://doi.org/10.1134/S1069351309050024.

Lyubushin, A. A. (2010a). The statistics of the time segments of low-frequency microseisms: Trends and synchronization. *Izvestiya, Physics of the Solid Earth, 46*(6), 544–554. https://doi.org/10.1134/S1069351310060091.

Lyubushin, A. (2010b). Multifractal parameters of low-frequency microseisms, in Synchronization and Triggering: From Fracture to Earthquake Processes. In V. de Rubeis, et al. (Eds.), *GeoPlanet: Earth and planetary sciences* (Vol. 1, pp. 253–272). Berlin: Springer. https://doi.org/10.1007/978-3-642-12300-9_15. **(Chapter 15)**.

Lyubushin, A. A. (2011). Cluster analysis of low-frequency microseismic noise. *Izvestiya, Physics of the Solid Earth, 47*(6), 488–495. https://doi.org/10.1134/S1069351311040057.

Lyubushin, A. (2012). Prognostic properties of low-frequency seismic noise. *Natural Science, 4*(8A), 659–666. https://doi.org/10.4236/ns.2012.428087.

Lyubushin, A. (2013). How soon would the next mega-earthquake occur in Japan. *Natural Science, 5*(8), 1–7. https://doi.org/10.4236/ns.2013.58A1001. **(A1)**.

Lyubushin, A. A. (2014a). Dynamic estimate of seismic danger based on multifractal properties of low-frequency seismic noise. *Natural Hazards, 70*(1), 471–483. https://doi.org/10.1007/s11069-013-0823-7.

Lyubushin, A. A. (2014b). Analysis of coherence in global seismic noise for 1997–2012. *Izvestiya, Physics of the Solid Earth, 50*(3), 325–333. https://doi.org/10.1134/S1069351314030069.

Lyubushin, A. A. (2015). Wavelet-based coherence measures of global seismic noise properties. *Journal of Seismology, 19*(2), 329–340. https://doi.org/10.1007/s10950-014-9468-6.

Lyubushin, A. (2018a). Synchronization of geophysical fields fluctuations. In T. Chelidze, L. Telesca, & F. Vallianatos (Eds.), *Complexity of seismic time series: Measurement and applications* (pp. 161–197). Amsterdam: Elsevier. https://doi.org/10.1016/B978-0-12-813138-1.00006-7. **(Chapter 6)**.

Lyubushin, A. (2018b). Global coherence of GPS-measured high-frequency surface tremor motions. *GPS Solutions, 22,* 116. https://doi.org/10.1007/s10291-018-0781-3.

Lyubushin, A. A. (2018c). Cyclic properties of seismic noise and the problem of predictability of the strongest earthquakes in Japanese Islands. *Izvestiya, Atmospheric and Oceanic Physics, 54*(10), 1460–1469. https://doi.org/10.1134/S0001433818100067.

Mallat, S. (1999). *A wavelet tour of signal processing* (2nd ed.). San Diego: Academic Press.

Marple, S. L., Jr. (1987). *Digital spectral analysis with applications*. Englewood Cliffs: Prentice-Hall Inc.

McNamara, D. E., & Buland, R. P. (2004). Ambient noise levels in the continental United States. *Bulletin of the Seismological Society of America, 2004*(94), 1517–1527.

Nicolis, G., & Prigogine, I. (1989). *Exploring complexity, an introduction*. New York, NY: W.H. Freedman and Co.

Nishida, K., Kawakatsu, H., Fukao, Y., & Obara, K. (2008). Background Love and Rayleigh waves simultaneously generated at the Pacific Ocean floors. *Geophysical Research Letters, 35,* L16307.

Nishida, K., Montagner, J., & Kawakatsu, H. (2009). Global surface wave tomography using seismic hum. *Science, 326*(5949), 112.

Pavlov, A. N., & Anishchenko, V. S. (2007). Multifractal analysis of complex signals. *Physics—Uspekhi Fizicheskikh Nauk, Russian Academy of Sciences, 50*(8), 819–834. https://doi.org/10.1070/PU2007v050n08ABEH006116.

Ramirez-Rojas, A., Munoz-Diosdado, A., Pavia-Miller, C. G., & Angulo-Brown, F. (2004). Spectral and multifractal study of electroseismic time series associated to the M_w = 6.5 earthquake of 24 October 1993 in Mexico. *Natural Hazards and Earth System Sciences, 4*(2004), 703–709.

Rhie, J., & Romanowicz, B. (2004). Excitation of Earth's continuous free oscillations by atmosphere–ocean–seafloor coupling. *Nature, 2004*(431), 552–554.

Rhie, J., & Romanowicz, B. (2006). A study of the relation between ocean storms and the Earth's hum. *Geochemistry, Geophysics, Geosystems*. https://doi.org/10.1029/2006GC001274.

Sarlis, N. V., Skordas, E. S., Mintzelas, A., & Papadopoulou, K. A. (2018). Micro-scale, mid-scale, and macro-scale in global seismicity identified by empirical mode decomposition and their multifractal characteristics. *Scientific Reports., 8,* 9206. https://doi.org/10.1038/s41598-018-27567-y.

Schimmel, M., Stutzmann, E., Ardhuin, F., & Gallart, J. (2011). Polarized Earth's ambient microseismic noise. *Geochemistry, Geophysics, Geosystems, 12,* Q07014.

Stehly, L., Campillo, M., & Shapiro, N. M. (2006). A study of the seismic noise from its long-range correlation properties. *Journal of Geophysical Research, 111,* B10306.

Tanimoto, T. (2001). Continuous free oscillations: Atmosphere–solid earth coupling. *Annual Review of Earth and Planetary Sciences, 29,* 563–584.

Tanimoto, T. (2005). The oceanic excitation hypothesis for the continuous oscillations of the Earth. *Geophysical Journal International, 160,* 276–288.

Taqqu, M. S. (1988). *Self-similar processes* (Vol. 8, pp. 352–357)., Encyclopedia of statistical sciences New York, NY: Wiley.

Telesca, L., Colangelo, G., & Lapenna, V. (2005). Multifractal variability in geoelectrical signals and correlations with seismicity: A study case in southern Italy. *Natural Hazards and Earth System Science, 5,* 673–677.

Telesca, L., & Lovallo, M. (2011). Analysis of the time dynamics in wind records by means of multifractal detrended fluctuation analysis and the Fisher–Shannon information plane. *Journal of Statistical Mechanics: Theory and Experiment*. https://doi.org/10.1088/1742-5468/2011/07/P07001.

Varotsos, P. A., Sarlis, N. V., & Skordas, E. S. (2003a). Long-range correlations in the electric signals that precede rupture: Further investigations. *Physical Review E, 67,* 021109. https://doi.org/10.1103/PhysRevE.67.021109.

Varotsos, P. A., Sarlis, N. V., & Skordas, E. S. (2003b). Attempt to distinguish electric signals of a dichotomous nature. *Physical Review E, 68,* 031106. https://doi.org/10.1103/PhysRevE.68.031106.

Varotsos, P. A., Sarlis, N. V., & Skordas, E. S. (2011). *Natural time analysis: The new view of time. Precursory seismic electric signals, earthquakes and other complex time series*. Berlin: Springer. https://doi.org/10.1007/978-3-642-16449-1.

Zotov, L., Bizouard, C., & Shum, C. K. (2016). A possible interrelation between Earth rotation and climatic variability at decadal time-scale. *Geodesy and Geodynamics, 7*(3), 216–222. https://doi.org/10.1016/j.geog.2016.05.005.

Zotov, L., Sidorenkov, N. S., Bizouard, C., Shum, C. K., & Shen, W. (2017). Multichannel singular spectrum analysis of the axial atmospheric angular momentum. *Geodesy and Geodynamics, 8*(6), 433–442. https://doi.org/10.1016/j.geog.2017.02.010.

(Received June 13, 2019, revised September 13, 2019, accepted September 18, 2019)